Influence of droplet deformability on the coalescence rate of emulsions

Jhoan Toro-Mendoza,* Aileen Lozsan, Maximo Garcia-Sucre, Aly J. Castellanos S., and German Urbina-Villalba
Centro de Estudios Interdisciplinarios de la Física, Instituto Venezolano de Investigaciones Científicas (IVIC), Caracas 1020A, Venezuela
(Received 10 March 2009; revised manuscript received 1 November 2009; published 13 January 2010)

In this article the influence of deformation on the coalescence rates of oil-in-water (O/W) emulsions is analyzed. Calculations for doublets and many-particles systems were performed based on a Brownian dynamics algorithm. Extensional and bending energies were included in order to quantify the effect of the changes in the surface geometry on the coalescence rates. Also, the hydrodynamic resistance due to the flat film was included through a correction to the diffusion coefficient in the lubrication limit. Results of two particles calculations were compared with previous analytical evaluations of the coalescence time in absence of highly repulsive barriers [Danov *et al.*, Langmuir **9**, 1731 (1993)]. Lifetime of doublets was calculated as a function of the particle radius from 100 nm to 100 μm. It was found that the doublets lifetime strongly depends on the interplay between the potential of interaction between the droplets and the hydrodynamic resistance. Depending on the repulsive barrier either a monotonous increase of the lifetime with the droplet size or a maximum value is observed. Finally, the evolution of O/W emulsions with a volume fraction of ϕ=0.10 was studied. For these many-particle systems, the results show a sensitive dependence of the aggregation behavior on the interfacial tension. The procedure reported here allows us to include Derjaguin-Landau-Verwey-Overbeek (DLVO) and non-DLVO forces and the film drainage velocity of many different systems.

DOI: 10.1103/PhysRevE.81.011405 PACS number(s): 82.70.Kj, 83.10.Mj, 47.57.Bc, 47.55.D−

I. INTRODUCTION

External forces and viscous stresses can deform the surface of emulsion droplets [1]. During a collision, the intervening liquid film between the droplets resists to drain, exerting a net tangential force on their surfaces leading to a surface deformation. As a consequence, the coalescence of droplets (the main mechanism of phase separation in emulsions) is dominated by the film thinning and the stability of emulsions is clearly affected by the surface deformation [2]. The flattening of the surface increases both the hydrodynamic resistance and the magnitude of the interparticle interactions (van der Waals, electrostatic, steric, etc.) Besides, two additional energies appear as a consequence of the augment of the surface area and curvature, namely, the extensional and bending energy, respectively [3]. The aim of this work is to analyze the effect of droplet deformability on the coalescence rates of oil-in-water emulsions.

It is often difficult to establish a direct relation between the surface properties of the droplets and the stability of the emulsion. This is mainly due to the following: (1) emulsions undergo many simultaneous processes, like flocculation, coalescence, creaming and Ostwald-ripening; (2) all of these processes are influenced by the time-dependent surfactant partition; (3) the interaction forces between the drops and their hydrodynamic resistance depend on the surfactant adsorption to the oil/water interface; and (4) as the droplet size change the viscoelastic surface properties vary as well. As a result of all this complexity, the prediction of stability is still limited to a restricted set of systems where either Derjaguin-Landau-Verwey-Overbeek (DLVO) or gravitational forces dominate. Many modifications to the Smoluchowski theory (developed for solid suspensions) [4–6] were necessary to include surface forces and hydrodynamic interactions [7–16] and to account for the surface fluidity and deformability [17,18]. Recently, a detailed tracing of the film profile and the coalescence time of two colliding droplets was studied [19]. The film was modeled as a cylindrical virtual particle with simultaneous variation of radius and thickness. The effect of the interfacial mobility on the coalescence time of deformable droplets was also considered.

In previous works, we performed emulsion stability simulations (ESS) based on a Brownian dynamics algorithm. In those articles the time evolution of oil/water/surfactant emulsions of nondeformable droplets subject to different physicochemical conditions was reported (see for instance Refs. [20,21]). In the present paper the results of the inclusion of droplet deformability in ESS are shown, based on a three-stages model which assumes that the drainage time is mainly spent in the thinning of the plane parallel film. A truncated spheres geometry was adopted to calculate the interaction forces between the particles. Besides, van der Waals, extensional, and bending energies were taken into account in the dynamics in order to quantify the effect of the energies associated to changes in the geometry on the coalescense rate. These computational conditions are compatible with a DLVO potential at high ionic strength.

The paper is divided as follows: next section is a revision of some advances in the knowledge of emulsion films and interactions between deformable droplets, in Sec. III the numerical procedure proposed is explained, Sec. IV deals with the results and discussion section, and finally the conclusions.

II. THEORETICAL AND EXPERIMENTAL BACKGROUND

A. Film formation and drainage

The close approach between two deformable emulsion droplets leads to the formation of a thin solvent film. This

*Also at Department of Chemical and Nuclear Eng., University of New Mexico; jtorom@ivic.ve

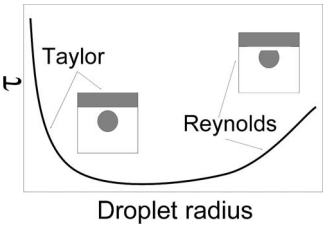

FIG. 1. Schematic illustration of the variation of the critical time vs. droplet radius obtained experimentally by Basheva *et al.* [35] for a system of one droplet coalescing with a planar liquid interface by effect of the buoyancy force. Two regimes are observed: the one of small droplets behaving as spheres (micron-sized droplets) and the one of larger droplets behaving as planar disks (millimetric-sized droplets).

process is governed by direct thermodynamic (van der Waals, electrostatic, etc.) and hydrodynamic interactions. The film drainage is determined by the action of these forces, following six main stages: (1) close approach between two slightly deformed drops; (2) inversion of the curvature sign in the contact zone, forming a dimple; (3) the dimple reaches the maximum depth and, under the action of the internal pressure, it starts to diminish until forming a plane film which drains; (4) the surface waves produced by thermal and hydrodynamic perturbations increase their amplitude due to attractive interactions between the particles leading to coalescence or, (5) the formation of thin spots called common black films (CBF) occurs, (6) convergence of the spots forming a single stable film known as Newton black film (NBF) [22].

The drainage and stability of films of micro and millimetric radii follows the stages outlined above. Other complex phenomena such as pimple formation [23], and the random nature of the processes leading to the NBF instability [24] are still being under study [25].

The earliest works focused on the mechanisms related with the rupture of liquid films. The seminal papers of Scheludko [26], Vrij [27,28], and Vrij and Overbeek [29] established a theoretical basis to relate the fluctuations responsible for the rupture to the molecular interactions across the film. They found expressions for the critical thickness of rupture, and the corresponding life time of such a process. For a film interacting with a van der Waals potential only, the equation for the critical distance reads [30]

$$h_{crit} = \left(\frac{A_H \lambda_{crit}^2}{128\gamma} \right)^{1/4}, \tag{1}$$

where A_H is the Hamaker constant, λ_{crit} is the critical surface wave amplitude and γ is the interfacial tension. In the Eq. (1) λ_{crit} is not directly determined from theory. According to experimental estimations $\lambda_{crit} \approx r_{mf}/10$, r_{mf} being the maximum film radius [30]. Other sophisticated theories were developed to include the effect of surface diffusion on the wave-induced drainage. They describe the hole formation probability for a nonhomogeneous surface distribution of surfactant [30–33]. However, the high internal pressure of micron-sized droplets prevents the formation of spots. Therefore, the mechanism responsible for the coalescence process in these systems is the drainage of the film [19].

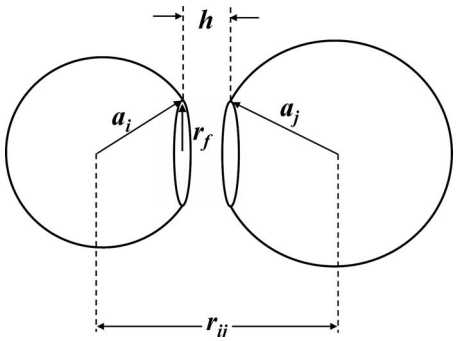

FIG. 2. Truncated spheres model for two deformed droplets of different radii a_i and a_j.

The critical time at which the film breaks is calculated by [22]

$$\tau = \int_{h_{crit}}^{\infty} \frac{dh}{V}, \tag{2}$$

here, V is the velocity of drainage of the film, h is the film thickness, and h_{crit} is the distance of rupture. In order to solve Eq. (2) the analytical expression for the velocity of drainage V is required. One of the first derivations was forwarded by Reynolds for the case of two rigid parallel disks [34]

$$V_{Re} = \frac{2Fh^3}{3\pi\eta r_f^4}, \tag{3}$$

where, η is the film viscosity, and r_f the film radius and F the external force acting on the disks. This equation was derived using the lubrication approximation and is the simplest model of droplet deformability. It considers the strong effect of the flat zone on the hydrodynamic resistance.

The dependence of τ on F was verified for the case of a droplet coalescing with a planar interface [35,36], as is shown schematically in Fig. 1. For the small particles, the time for coalescence τ diminishes as the particle radius increases along with the buoyancy force and the droplets behave as two approaching spheres [Taylor regime $V_{Tay} = 2hF/(3\pi\eta r_f^2)$]. Nevertheless, for larger particle radii, the coalescence time starts to grow as the particle radius increases because of the appearance of a planar disk at the surface of the droplet. Though for larger particles the buoyancy force is proportionally higher, the hydrodynamic resistance also increases by the flat deformation and becomes dominant. This regime follows the prediction made by the Reynolds equation.

A deduction of the thickness at which the curvature changes sign was made by Ivanov *et al.* in Ref. [37]. By using the lubrication approximation they obtained

$$h_0 = \frac{F}{2\pi\gamma}. \tag{4}$$

The distance h_0 is also known as the distance at which the droplets initiate the process of deformation. Danov *et al.*

reported an analytical expression for h_0 considering the case in which the total force on a particle suspended in a viscous medium is the result of two contributions: the Brownian force $[k_BT\nabla(\ln P)$, with P being the probability function] and the direct molecular interactions between the particles $(-\nabla W)$ [17]. Thus, the Eq. (4) was modified according to

$$h_0 = \frac{k_B T}{2\pi\gamma(f_d + f_f)}\epsilon_S, \tag{5}$$

where, k_B is the Boltzmann constant, T the temperature, ϵ_S a emulsion parameter with values between 1 (for tangentially immobile interfaces) and 0.001 (for pure liquids or for systems where the surfactant is only soluble in the disperse phase), f_d a factor which account for the region of deformation and f_f a term related to the film thinning region (see Fig. 1 in Ref. [17]). The latter dimensionless factors are given by integrals containing geometric factors and interaction energies. A model of two equal truncated spheres was used by the authors to calculate numerically h_0.

Danov *et al.* proposed the following scheme to model the deformation process of two colliding droplets [38]: (1) the particles start to deform at a surface-to-surface distance h_0, (2) the film starts to grow from $r_f=0$ up to $r_{mf}=\sqrt{ah_0}$ at constant surface-to-surface distance $h=h_0$, and, finally, (3) the film drains at constant film radius $r_f=r_{mf}$ until it reaches the critical distance $h=h_{crit}$ at which the droplets coalesce. This model is based on the assumption that most of the time to complete the six-stages process described above is mainly spent at stage 3, i.e., the drainage of the planar film. In addition, it incorporates the spherical part of the droplets which was neglected in the previous treatments, e.g., the Reynolds approximation. Denkov *et al.* [39,40] demonstrate that the contribution of the actual shape of the transition zone between the flat and the spherical part of the particle to the interaction potential can be neglected. Therefore, after deformation the droplets can be modeled as two truncated spheres, as shown in Fig. 2.

B. Interactions between droplets

The interactions between colloidal particles is generally studied within the framework of Derjaguin-Landau-Verwey-Overbeek theory (DLVO) [3]. This theory accounts for the attractive van der Waals force between the particles and a repulsive electrostatic interaction caused by surfactant adsorption and/or surface charges. It is now well established that steric, hydration, hydrodynamic, and depletion forces can strongly affect the stability and structure of the suspended particles. Additionally, the viscoelasticity of the droplets affects the interactions due to the changes of the surface geometry occurring during the deformation, The latter lead to the appearance of two additional energy contributions, i.e., increase of surface area and bending. On the other hand, hydrodynamic resistance grows as the flat zone extends.

Following a truncated sphere model for drop deformation (see Fig. 2) and using the Hamaker approach, Danov *et al.* obtained the van der Waals potential between two droplets of radii a_i and a_j, interacting with a Hamaker constant A_H [38],

$$\begin{aligned} W_{VW} = -\frac{A_H}{12}\Bigg(& \frac{2a_2(l_1-h)}{l_1(l_2+h)} + \frac{2a_2(l_1-h)}{h(l_1+l_2)} + 2\ln\left(\frac{h(l_1+l_2)}{l_1(h+l_2)}\right) + \frac{r_f^2}{h^2} - \frac{l_1-h}{l_2}\frac{2r_f^2}{hl_1} - \frac{l_1-a_1-(l_2-a_2)}{2l_1-2a_1-h}\frac{2r_f^2}{hl_1} - \frac{2(l_2-a_2)-h}{2l_1-2a_1-h}\frac{d-h}{2h} \\ & + \frac{2a_2l_2^2(l_1-h)}{hl_1(l_1+l_2)(l_2+h)} - \frac{2a_2^2}{h(2l_1-2a_1-h)}\frac{l_1^2+r_f^2}{(l_1+l_2)(l_1+l_2-2a_2)} \\ & + \frac{2a_2^2 d}{(2l_1-2a_1-h)[(h+l_2)(h+l_2-2a_2)-(l_1-h)(l_1-2a_1-h)]} \\ & - \frac{4a_2^3(l_1-h)}{[(h+l_2)(h+l_2-2a_2)-(l_1-h)(l_1-2a_1-h)]}\frac{1}{(l_1+l_2)(l_1+l_2-2a_2)}\Bigg), \end{aligned} \tag{6}$$

where $l_1=h+a_1+\sqrt{a_1^2-r_f^2}$, $l_2=a_2+\sqrt{a_2^2-r_f^2}$, and $d=\sqrt{h^2+4r_f^2}$. For $r_f=0$ the expression for two spheres is recovered. Explicit expressions for electrostatic, steric, and depletion interactions were derived by using the Derjaguin approximation. The calculations indicate an increment of the magnitude of each contribution to the interaction potential due to the presence of a planar zone which was confirmed experimentally [41].

In addition, two contributions to the mechanical work arise. They are due to the increment in surface area $(\gamma\delta A)$ and in the surface curvature $(B\delta H)$, where A is the surface area, B the interfacial bending moment, and H the interfacial curvature [42]. For a deformed droplet (according to Fig. 2), the contribution from the increment of surface area is given by

$$W_E = \int_{sphere}^{deformed} \gamma(S)dS, \tag{7}$$

where S is the area of the deformed surface. Assuming a constant interfacial tension, the Gibbs elasticity can be neglected. Based on this approximation and for small deforma-

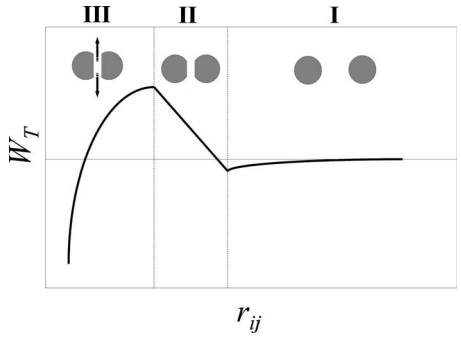

FIG. 3. Interaction potential between two deformable droplets according to the three-stages collision model: (i) the droplets keep spherical until reaching a surface-to-surface distance h_0. (ii) the film starts to grow at constant separation thickness. (iii) The film reaches the maximum radius and starts to drain.

tions ($r_f/a \ll 1$), Danov *et al.* obtained the extensional energy for two slightly deformed droplets of equal radius [38],

$$W_E = \frac{\pi \gamma r_f^4}{2a^2}. \tag{8}$$

The positive value of W_E represents a "repulsive" energy between the colliding droplets. As can be seen, the extensional contribution to the energy is proportional to γ. The change in the interfacial curvature can be considered as an additional degree of freedom [42] which can be expressed in terms of differences of the droplet curvature energy after and before the film formation [40], i.e.,

$$W_B = -2\pi r_f^2 B_0 H\left(1 - \frac{H}{2H_0}\right), \tag{9}$$

where H_0 is the spontaneous curvature and B_0 the bending moment of a planar surface. For emulsion droplets, the term $H/2H_0$ can be neglected since the curvature of the droplet is several times smaller than H_0 ($H \sim 10^{-3}$ nm^{-1} and $H_0 \sim 1$ nm^{-1}). This simplifies Eq. (9), for $(r_f/a)^2 \ll 1$,

$$W_B = -\pi r_f^2 \frac{B_0}{\bar{a}}. \tag{10}$$

with $1/\bar{a} = 1/a_i + 1/a_j$. For O/W emulsion B_0 opposes to flattening unlike the case of W/O emulsions, where the flattening is favored. The sign of B_0 and H are conveniently chosen to be in agreement with this fact. The theoretical value of B_0 for oil/water interfaces is $\sim 5 \times 10^{-11}$ N. This is calculated from the van der Waals and electrostatic contributions to the bending moment. For emulsion droplets radii between 1 and 100 microns, the bending energy changes between 2 and 200 k_BT, contrary to the general belief that the bending energy affects only nanometric droplets and microemulsions [43].

Figure 3 illustrates the behavior of the total potential energy ($W^T = W_{vdW} + W_E + W_B$) with the center-to-center distance r_{ij}. This potential was calculated adopting the three-stages model for the collision of two deformable O/W droplets mentioned at the end of Sec. II A. The droplets are spherical until reaching a distance h_0 between surfaces. At this separation they interact via van der Waals forces (zone I in figure). Then, the film radius evolves from $r_f = 0$ to $r_f = r_{mf} = \sqrt{ah_0}$. The value of r_{mf} was derived by Ivanov *et al.* [37] and corresponds to the dimple radius. In this zone (II in Fig. 3), the particles approach each other at constant surface-to-surface separation $h = h_0$ where the bending and extensional energies rise as the film radius increases. Finally, in the zone III the film radius have reached its maximum value r_{mf} and the film drains until reaching a distance $h = h_{crit}$ where the droplets coalesce. In that zone, the values of W_E and W_B remain constant. Hence, they do not contribute to the total force. As can be seen in Fig. 3, the deformation can generate a barrier that prevents or delays the coalescence.

C. Effect on emulsion stability

The surface deformability of the droplets plays a major role in the stability of emulsions [44,45]. Hofman and Stein reported differences in the stability of decane-in-water emulsion stabilized with aerosol-OT (the sald of di-octyl-sulphosuccinic acid) and sodium oleate NaOl which are between two and four orders of magnitude [2] (see Fig. 2 therein). These two systems show a similar electrostatic repulsion and Hamaker constant ($A_H = 1.1 \times 10^{-20}$ J). However, the interfacial tension of the AOT system reaches ultralow values at high ionic strength while that of NaOl is 0.1mN/m. The authors argue that the deformation is responsible for these differences in stability.

Other experimental works considered the deformability as a repulsive contribution to the total interaction energy between weakly charged emulsions particles [46,47]. It was shown that the deformability leads to a stronger flocculation, since the attractive energy becomes significant due to the presence of a planar film in the contact zone, resulting in a coalescence instability of the system [48]. A previous analytical work predicts small differences between the coalescence rate of nondeformable and deformable droplets, arguing that small droplets barely deform and large droplets coalesce as fast as spheres due to the increase in the van der Waals energy resulting from the deformation [17]. More recently, nanoemulsion studies have suggested the importance of the effect of deformability, despite the high internal pressure of the droplets [49,50]. This behavior makes necessary to revisit the possible correction of the interfacial tension value with the curvature (see for instance Ref. [51]). New studies suggest possible effect of droplet deformation on the emulsion rheology [52]. In a review on the effect of deformability on micron-size emulsion droplets, Ivanov *et al.* summarized the factors which make possible the flattening of the contact zone and the consequences on the particles collision [53].

III. ACCOUNTING FOR DROPLET DEFORMABILITY IN EMULSION STABILITY SIMULATIONS

Brownian dynamics allow to include the approximations mentioned in the previous section and to follow the time evolution of emulsions, evaluating from output data the destabilization rates and aggregation behavior as well [54–57].

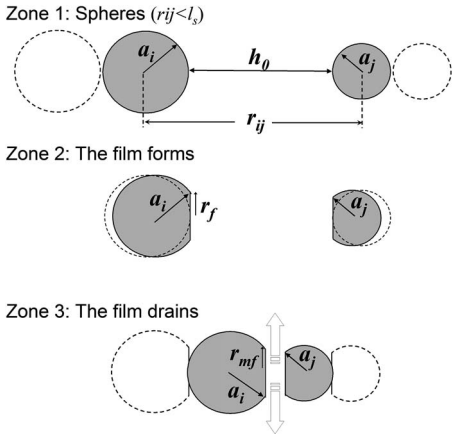

FIG. 4. Definition of h and r_f depending on the separation r_{ij} used in order to introduce them in equations for W and D, following the three-stages deformation process model. Distances and droplet deformation were exaggerated for a better visualization.

The article of Ermak and McCammon [58] forward the most common algorithm used for Brownian dynamic simulations of solid spheres. A simplified equation of motion is [21,59]

$$\mathbf{r}_i(t+\Delta t)-\mathbf{r}_i(t)=\frac{D_i^{corr}\mathbf{F}_i}{k_BT}\Delta t+\mathbf{R}(\Delta t), \tag{11}$$

where $\mathbf{r}_i$ is the position of the i-particle, D^{corr} is the "corrected" diffusion constant which reproduces the hydrodynamic interactions. It depends on the local volume fraction ϕ and the distance d to the closest neighbor particle [59], $\mathbf{F}_i$ is the total force on the i particle (interparticle and external forces), Δt the time step, and $\mathbf{R}$ the random term representing the Brownian motion with zero mean and variance $6D_i\Delta t$.

Emulsion stability simulations start from a cubic box that contains N drops randomly distributed. The particles move according to Eq. (11). In previous works the space around each particle was divided in three regions [59] in order to account for hydrodynamic interaction between spherical droplets. If at least one j-particle reaches the internal region $r_{ij}<l_s$, the exact formula of Honig *et al.* is used to compute the diffusion constant of i. Otherwise the volume fraction ϕ of particles around i is used to evaluate an empirical expression of $D^{corr}(\phi)$ [60]. Particles located at $r_{ij}>R_{ext}$ do not contribute to the hydrodynamic effects on i (see Ref. [59] for more details).

In this work droplet deformation was modeled as explained at the end of Sec. II A. Thus, for the evaluation of F and D we introduce three new "zones" inside the region defined by $r_{ij}<l_s$, as is shown in Fig. 4: (1) interparticle surface distances larger than h_0, droplets are spheres (zone 1), (2) interparticle surface distances less than h_0, droplets centers approach at constant surface separation $h=h_o$, but film radius evolves from $r_f=0$ to $\sqrt{ah_o}$ (zone 2), and (3) film thickness thins at constant film radius until it reaches the critical distance h_{crit}, calculated from Eq. (1) (zone 3).

To determine h_0, a polynomial expression was fitted to curves obtained in Ref. [17] (see Fig. 2.7, curve labeled 2 therein). The resulting adjust for interfacial tension and droplet radius parameters lead us to

$$h_0=(1.2932\times10^{-8}-8.6475\times10^{-9}e^{-a_i/1.8222\times10^{-6}})\times\frac{3.3253\times10^{-9}+5.9804\times10^{-9}e^{-\gamma/0.00402}}{3.3253\times10^{-9}+5.9804\times10^{-9}e^{-1\times10^{-3}/0.00402}}. \tag{12}$$

Equation (12) is meant to generate an approximate value of h_0 (in meters) with the correct theoretical tendency on a_i and γ.

In order to derive the interparticle forces ($F_{ij}=-\partial W/\partial r_{ij}$) from the Eqs. (6), (8), and (10), the variables r_f and h were substituted. The values of these variables depend on interparticle center distances r_{ij}, and can be calculated by trigonometry according to (see Fig. 4):

(1) *Zone 1:* Spherical droplets. For $r_{ij}>a_i+a_j+h_0$,

$$r_f=0;\quad h=r_{ij}-(a_i+a_2). \tag{13}$$

(2) *Zone 2:* at constant surface-to-surface distance, the film radius grows from $r_f=0$ to $r_{mf}=\sqrt{ah_0}$. For $h_0+(\sqrt{a_i^2-a_ih_0}+\sqrt{a_j^2-a_ih_0})<r_{ij}<a_i+a_j+h_0$,

$$r_f=\sqrt{a_i^2-\left[\left(\frac{a_i}{a_i+a_j}\right)(r_{ij}-h_0)\right]^2};\quad h=h_0. \tag{14}$$

(3) *Zone 3:* at constant maximum film radius $r_{mf}=\sqrt{ah_0}$, drainage occurs until reaching the critical coalescence distance h_{crit}. For $h_{crit}+(\sqrt{a_i^2-a_ih_0}+\sqrt{a_j^2-a_ih_0})<r_{ij}<h_0+(\sqrt{a_i^2-a_ih_0}+\sqrt{a_j^2-a_ih_0})$,

$$r_f=r_{mf}=\sqrt{a_ih_0};\quad h=r_{ij}-\sqrt{a_i^2-r_{mf}^2}-\sqrt{a_j^2-r_{mf}^2}. \tag{15}$$

The film radius r_f formed between two droplets was calculated by using the parameters of the smaller one. The Hamaker constant also depends on the distance between the particles, because of the retardation effects. This can be included within the procedure shown here by evaluating the appropriate expression.

The diffusion coefficient of the deformed droplets was calculated in the lubrication limit. Based on this, we used a correction suggested by Petsev which accounts for the surface mobility ϵ_s of a truncated sphere [61]. The effective friction coefficient between to deformed droplets is

$$\zeta_{TS}=\zeta_{hh}+(1-\epsilon_s)\zeta_{r_fh}\frac{r_f}{2h}, \tag{16}$$

where the components hh and r_fh of the friction tensor are given by [18]

$$\zeta_{hh}=\frac{3\pi\eta a^2}{2h}\left(1+\frac{r_f^2}{ah}+\frac{r_f^4}{a^2h^2}\right), \tag{17}$$

$$\zeta_{r_fh}=-\frac{3\pi\eta r^3}{h^2}. \tag{18}$$

Using the general relations $D=k_BT/\zeta$, $\zeta=F/V$, the effective diffusion coefficient then reads

TABLE I. Critical parameters (in nanometers) for different droplet radii. Distances and film radius were calculated from Eqs. (1) and (12), respectively, and $r_{mf}=\sqrt{ah_0}$.

Droplet radius	100 nm			10 μm			50 μm		
γ(mN/m)	h_0	h_{crit}	r_{mf}	h_0	h_{crit}	r_{mf}	h_0	h_{crit}	r_{mf}
1×10^{-2}	5.5	1.5	23.4	14.5	9.2	387.2	15.0	9.2	867.1
1	4.7	0.4	21.7	12.8	1.8	359.1	12.9	2.8	804.1
50	1.9	0.1	14.0	5.3	0.5	231.7	5.4	0.8	518.8

$$D_{TS}=4D_0\frac{h}{a}\left(1+\frac{r_f^2}{ah}+\frac{r_f^4}{a^2h^2}\epsilon_s\right)^{-1}. \tag{19}$$

Here, $D_0=k_BT/6\pi\eta a$ is the Stokes diffusion. For comparison purposes, another expression was also used to approximate the diffusion coefficient. It contains the circular plane film correction of Reynolds and the correction due to the spherical part obtained by Honig *et al.* [62]

$$D_{HR}=\frac{D_{Re}}{\beta}=4a_iD_0\frac{1}{\beta}\frac{h^3}{r_f^4}, \tag{20}$$

where D_{Re} is the Reynolds diffusion constant. Using Eq. (3) we obtain

$$D_{Re}=\frac{2k_BTh^3}{3\pi\eta r_f^4}=4D_0a\frac{h^3}{r_f^4}, \tag{21}$$

and $\beta\simeq\frac{6u^2+13u+2}{6u^2+4u}(u=h/a)$ is the Honig *et al.* factor [62]. Our code has more than ten possible analytical expressions for the calculation of the diffusion constant (see Table I of Ref. [1]). Finally, the distance at which the particle coalescence is calculated by means of Eq. (1). Then, a new droplet located at the center of mass of the two coalescing droplets is created with a radius $a=(a_i^3+a_j^3)^{1/3}$. It is possible that the Brownian displacement represented by the last term in Eq. (11) pushes the film below the critical value h_{crit}. In this case, the coalescence occurs and the same procedure above outlined is applied to generate the new droplet.

IV. RESULTS AND DISCUSSION

A. Film parameters and diffusion coefficient

Critical film parameters are summarized in Table I for some selected particle radii and interfacial tensions. In order to compare with the results reported in the literature for emulsion systems (see for example Refs. [2,63]) a Hamaker constant $A_H=1\times10^{-20}$ J was used. As expected, the larger particle radius and the lower interfacial tension, the more deformable the droplets are (larger r_{mf}). It should be noticed that at $\gamma=50$ mN/m, the thickness of the film formed, i.e., the distance h_0-h_{crit} is around a half of the value corresponding to the case of $\gamma=1$ mN/m. Besides, the value of h_{crit} is considerably lower, which means that the droplets are spherical until the they approach one another very closely. Compared with the case of $\gamma=1$ mN/m, the distance h_0-h_{crit} for the system with $\gamma=0.01$ mN/m is smaller. This is due to the dependence on γ and h_0. It might be expected that systems with very low interfacial tension are more affected by surface waves, producing coalescence times smaller than systems with a higher γ. This is also important for the range of action of the interaction potential, since it acts at a larger interparticle distance, depending on γ.

Figure 5 illustrates the dependence of the diffusion coefficients with the particle radius calculated at the maximum film deformation. It is observed that all coefficients decrease monotonically as the radius increases. The correction D_{TS} was calculated using a surface mobility equal to 0.1. This value corresponds to a droplet surface with less hydrodynamic resistance than $\epsilon_s=1$ (immobile surface). The other corrections do not depend on this parameter. This means that the surface is immobile in those cases. It is well known that surface mobility affects the velocity of thinning of the film because it modifies the boundary conditions [64].

Although the droplet becomes more deformable as it increases in size, the formation of a large plane film augments the van der Waals attraction considerably. The "repulsive" energy arising from bending and surface extension is not enough to compensate the increase of the attraction. Therefore, from the energy behavior one can expect that the bigger droplets will coalesce with a lower potential barrier. However, the hydrodynamic interactions play an important role in the collision dynamics. The interplay between those quantities is evident in the following results for doublets.

B. Coalescence time of two droplets of equal size

In this section doublets lifetime τ for a range of droplet radii between 100nm and 100 μm is shown. Following the

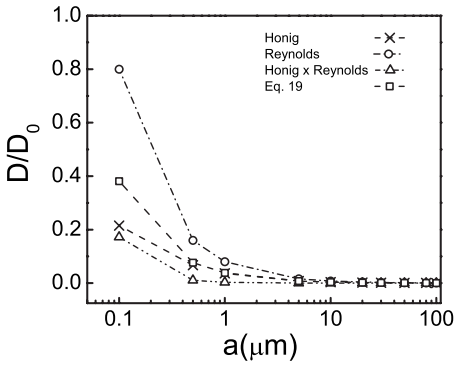

FIG. 5. Dependence of the different diffusion corrections on the size of droplet calculated according to Eqs. (19)–(21) and the Honig *et al.* correction ($D=D_0/\beta$). The values D/D_0 were calculated by using the maximum film deformation $r_{mf}=\sqrt{ah_0}$. Lines are a guide for the eyes.

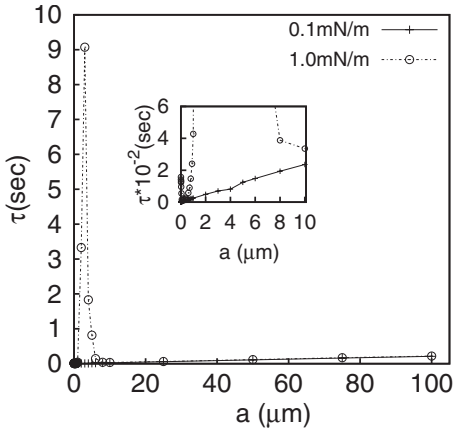

FIG. 6. Coalescence time of doublets of the same size. Correction to diffusion corresponds to Eq. (19).

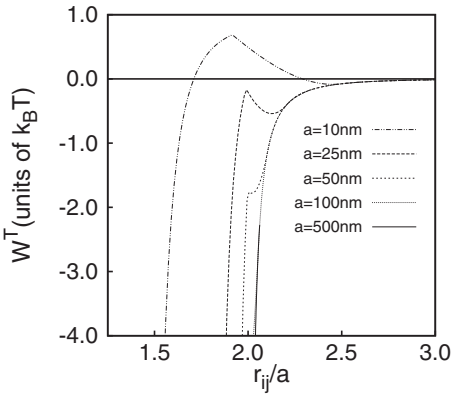

FIG. 8. Interaction potential for two deformable droplets of equal size. The interfacial tension is 0.1 mN/m.

suggestions of the reviewer, we validated the code comparing the results of two-particle simulations with the analytical evaluations of Ref. [17] using the correction proposed in Eq. (19). In their calculations, Danov *et al.* only used extensional (γ=0.1 mN/m) and van der Waals ($A_H=1\times10^{-20}$ J) potentials. The present version of the code can either simulate the behavior of nondeformable or deformable drops. Hence, it is the comparison of the simulations with the experiment that will determine the relevance of deformability or nondeformability in a particular system. The two colliding droplets have the same radius, and the initial position of the droplets corresponds to a surface-to-surface separation of h_0=20 nm. The values for the physical parameters used were $A_H=1\times10^{-20}$ J, γ=0.1 mN/m and 1 mN/m. The time step used was between 1.0×10^{-10} s and 5.1×10^{-3} s and 1000 numerical experiments were carried out for each radius by using a different seeds randomly generated at the first iteration. For this reason, the times shown are the average values calculated from those numerical experiments. Only extensional and van der Waals energies were considered in order to generate energy barriers $<2\ k_BT$, easily surpassed by the Brownian fluctuation. Otherwise, the particles would go apart from each other, diminishing the probability of the collision because of the dimension of the simulation box (more than 10 times the particle radius). For each set of computational conditions two simulations were run. The first one corresponds to nondeformable droplets, and the second one to deformable droplets. In the former case the hydrodynamic friction was calculated by means of the Stokes diffusion for $r_{ij}>a_i$ and the Honig correction (D_0/β) for $h_0\leq h\leq a_i$.

Figures 6 and 7 show the coalescence times obtained by using the correction to the diffusion calculated according to Eqs. (19) and (20), respectively. In our case, τ should be proportional but not equal to the lifetime of doublets of particles since the initial distance of separation (20 nm) is larger than the value of h_0 calculated from Eq. (12) (5–15 nm). As observed, the coalescence time predicted by Eq. (20) are significantly higher than the ones predicted by Eq. (19). For particles larger than 10 microns Eq. (20) produces a significant increase in the coalescence time with the particle radius, while the one proposed by Petsev only presents a moderate increase. Moreover, the diffusion corrected according Eq. (20) produces a variation of the stability ratios for $a>10$ μm (see below).

The free energy of surface extension produces a repulsive barrier acting as an effective repulsive potential. Hence, the movement of the drops depends on the balance between the effect of the hydrodynamic resistance and the interaction potential. For γ=0.1 mN/m the repulsive barrier produced by

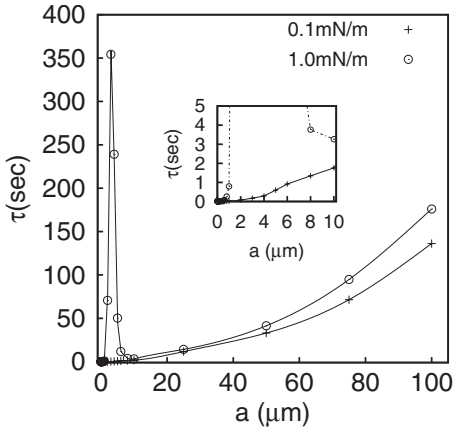

FIG. 7. Coalescence time of doublets of the same size. Correction to diffusion corresponds to Eq. (20).

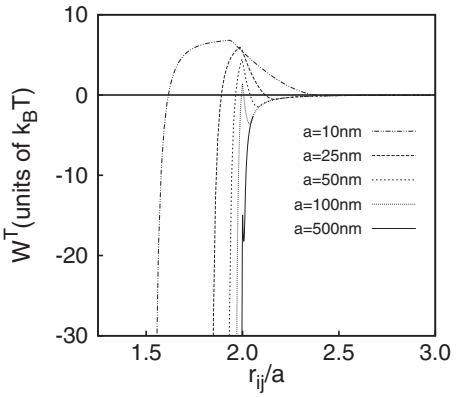

FIG. 9. Interaction potential for two deformable droplets of equal size. The interfacial tension is 1 mN/m. Droplet radius from 10 to 500 nm.

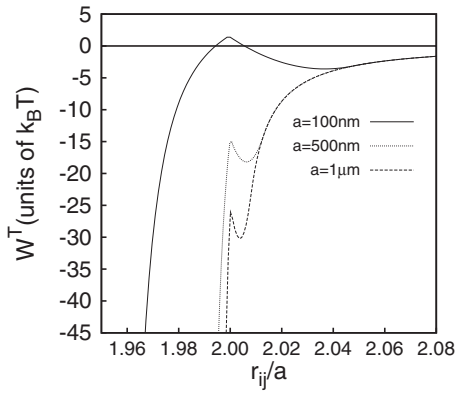

FIG. 10. Interaction potential for two deformable droplets of equal size. The interfacial tension is 1 mN/m. Droplet radius from 100 nm to 1 μm.

the extensional potential is small (Fig. 8). If the height of the repulsive barrier is estimated as the difference between the minimum value of the secondary minimum and the maximum value of the interaction potential barrier heights of 0.75 k_BT, 1.15 k_BT, and 0.01 k_BT are observed for pairs of particles with a radius of 10, 25, and 50 nm. The potential of interaction is negative for $a>25$ nm. As a result of this small potential, barriers the effect of the diffusion coefficient is decisive. The coalescence time increases progressively with the particle radius. According to Fig. 6, for instance, it never surpasses 0.25 s for 5 μm$\leq a\leq$100 μm.

For $\gamma=1$ mN/m the repulsive barrier produced by the extensional energy is significant (Figs. 9–11). Barriers heights of 6.6 k_BT, 5.3 k_BT, 5.8 k_BT, 5.0 k_BT, 3.8 k_BT, 3.8 k_BT, 5.3 k_BT, 9.1 k_BT, and 2.0 k_BT are obtained, for particle radii of: 10 nm, 25 nm, 50 nm, 100 nm, 200 nm, 500 nm, 1 μm, 3 μm, and 6 μm, respectively. The maximum of the potential is positive as $a<100$ nm (Fig. 9). For $a>6$ μm the repulsive barrier disappears and the total potential closely follows the shape of the van der Waals interaction. In this case, the effect of the interaction potential outweighs the drag produced by the hydrodynamic resistance. At small particle radius ($a<100$ nm), the potential barrier decreases with the particle radius. This causes a decrease of the coalescence time as a function of a. At intermediate particle radius (0.5 μm$\leq a\leq$6 μm) the potential of interaction is negative, but the height of the repulsive barrier increases, passes through a maximum and then decreases. This generates a peak of the coalescence time. The predictions of the diffusion correction (19) for this large particle radius coincide with the ones for spherical droplets. On the other hand, the tendency observed after the maximum value of τ is quite similar to the curve reported for coalescence of droplets and planar interfaces (see Fig. 1).

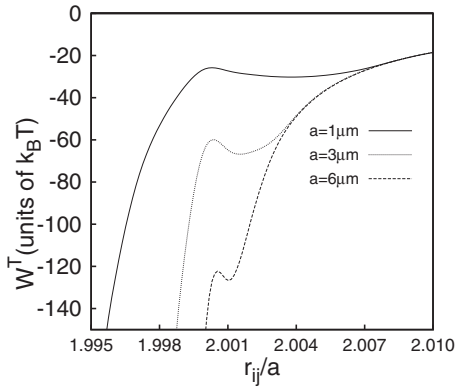

FIG. 11. Interaction potential for two deformable droplets of equal size. The interfacial tension is 1 mN/m. Droplet radius from 1 to 6 μm.

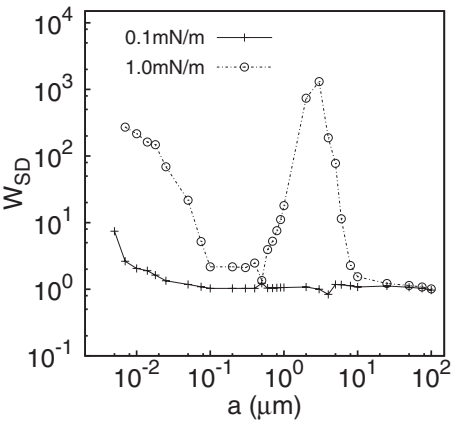

FIG. 12. Stability ratio W_{SD} estimated from calculations according to Eq. (22). The diffusion was calculated using Eq. (19).

Figures 12 and 13 show the stability ratio of deformable droplets W_{SD} calculated for the two corrections to the diffusion tested in this paper. In Ref. [17] the stability ratio of Fuchs was evaluated. That stability ratio does not account for the attraction between the particles. Besides, it compares the coalescence time between a couple of deformable particles with the behavior of two spheres executing Brownian motion. In the present case, the coalescence time of deformable droplets is compared with the behavior of two attractive spheres. The value of W_{SD} was estimated following the procedure outlined in Ref. [65],

$$W_{SD}=\frac{t_c^{dd}}{t_c^{s}}, \tag{22}$$

where superscripts *dd* and *s* stand for deformable drops and spheres, respectively. The value of W_{SD} for deformable sys-

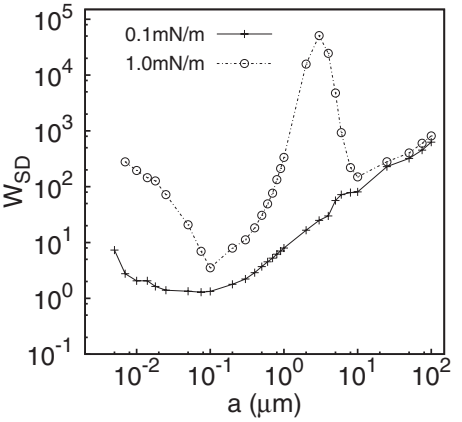

FIG. 13. Stability ratio W_{SD} estimated from calculations according to Eq. (22). The diffusion was calculated using Eq. (20).

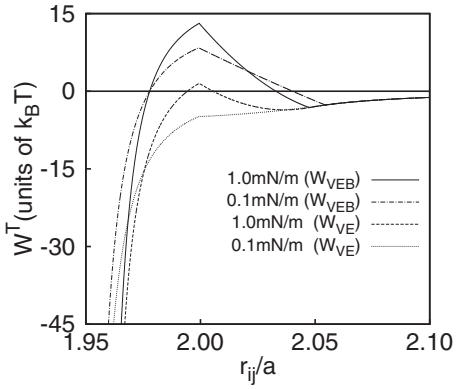

FIG. 14. Interaction potential between two droplets of 100 nm for two different interfacial tensions. Lower curves correspond to absence of bending energy.

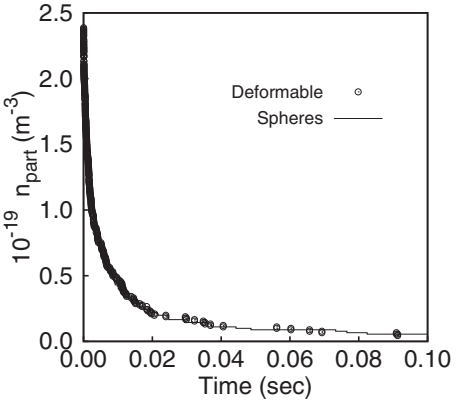

FIG. 16. Time evolution of the number of particles per unit volume of a system of $a=100$ nm and $W^T=W_{VE}$ ($\gamma=0.1$ mN/m).

tems was estimated using the diffusion of Stokes and either Eq. (19) or Eq. (20). The coalescence time of the spheres was evaluated using the diffusion of Stokes and the correction due to Honig *et al.* [62].

It is noticeable that in the absence of a repulsive potential ($a>6$ μm) ($\gamma=0.1$ mN/m) the correction D_{TS} shows a monotonous decrease in W_{SD} reaching the value of 1.0 at large particle radius (see Fig. 12). This means that the deformable drops behave as spheres if the potential is attractive or negligible. Instead, the presence of a significant potential barrier ($\gamma=1$ mN/m) produces a shape of the stability ratio curve that resembles the one exhibited by the coalescence time (Figs. 6 and 7). W_{SD} decreases at small particle radius, shows a maximum value around 3 microns, followed by a decrease, asymptotically tending to 1.0 for $a>10$ μm. The correction to the diffusion proposed by Eq. (20) produces a systematic increase of W_{SD} with the particle radius which is superimposed to the effect of the interaction potential.

In other words, the results of Ref. [17] are reproduced by our simulations as long as the repulsive potential between the drops is negligible. In this case, small drops behave as spherical particles. Moreover, the delay in the coalescence time produced by the deformation of large drops and the drainage of the intervening liquid film is counterbalanced by the increase of the attractive interaction due the change in the geometry of the drops. However, if a sizeable repulsive barrier exists, our calculations show striking differences in the behavior of deformable and nondeformable drops. In general, the average flocculation and coalescence rates decrease as a consequence of the deformation of the drops. In the present case, the repulsive barrier is originated by an increase in the interfacial tension, and/or the inclusion of the bending potential. Nevertheless, it is clear that any repulsive potential will favor this behavior.

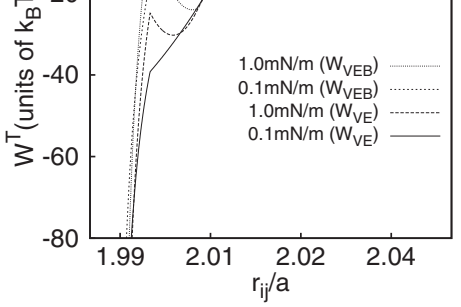

FIG. 15. Interaction potential between two droplets of 1 μm for two different interfacial tensions. Lower curves correspond to absence of bending energy.

C. Many-particles systems

It is clear from the results of the previous section that the extensional energy has a marked influence on the dynamics of a binary collision between deformable droplets. Similar results are obtained if the bending potential is included in the simulations. The difference in the behavior between spherical droplets and deformable droplets being most significant around $a=3$ μm.

In order to simulate the behavior of emulsions, $N=216$ particles were used. The drops were initially placed at random positions within a cubic box with a side length $L=20.84a$. A small volume fraction of internal phase was chosen ($\phi=0.10$) in order to disfavor the occurrence of many-particle collisions. The calculations were performed for two different interfacial tensions (0.1 and 1.0 mN/m) and two particle sizes: 100 nm and 1 μm. All simulations included the van der Waals attraction between the particles. Half of the calculations incorporated the extensional potential ($W_{VE}=W_{vdW}+W_E$) and the other half a combination of the extensional and the bending potential ($B_0=1.6\times10^{-12}$ N, $W_{VEB}=W_{vdW}+W_E+W_B$). The time step of the simulations was: $\Delta t=8.2\times10^{-9}$ s ($\sim4.1t_{Br}$) for $a=100$ nm, and $\Delta t=2.0\times10^{-6}$ s (~10.2 t_{Br}) for $a=1$ μm, where $t_{Br}=mD_0/k_BT$ and m is the mass of a droplet [58]. In all calculations, the correction (19) was employed. It is noticeable that we use this approximation to consider the surface mobility of the droplet which represent most of cases in emulsion systems [64]. Here, a value of $\epsilon_s=0.1$ was used.

Systems with a volume fraction of 0.10 contain $n_0=2.39\times10^{19}$ particles/m^3 for $a=100$ nm, and $n_0=2.39$

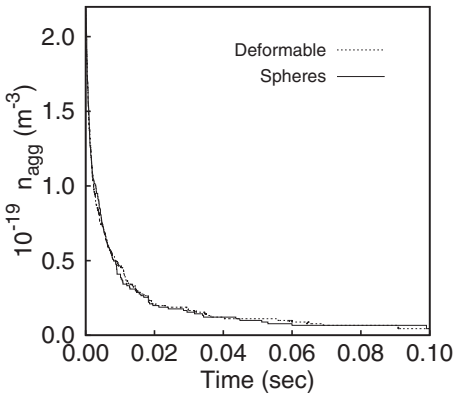

FIG. 17. Time evolution of the number of aggregates per unit volume of a system of $a=100$ nm and $W^T=W_{VE}$ ($\gamma=0.1$ mN/m).

$\times 10^{16}$ particles/m^3 for $a=1$ μm. While the variation of the number of particles is given directly by the simulations, the calculation of the number of aggregates requires further treatment of the data. A separate code uses the coordinate file produced by the simulations using a "flocculation distance" as input. The flocculation distance may vary considerably due to the polydispersity of the system and the characteristics of the interaction potential. In the case of deformable drops, the initial distance of deformation depends on the particle size, which increases during the simulation ($\sim$20 nm). The code reads the coordinates of the particles from the coordinate file of the simulations, and processes them for each time. First, it identifies the number of neighbors that stand at a distance $h<20$ nm, from the first particle. Then it repeats the same procedure for the particle's neighbors and its neighbors' neighbors, until no other new members of the floc appear. At this point the number of particles of the first aggregates was identified and can be stored. Following, the program erases the particles of the first floc from the set of coordinates, and repeats the procedure for the rest of the particles. When these computations finish, the new set of coordinates can be processed and so on.

Figure 14 illustrates the interaction potential between two drops of $a=100$ nm. Barrier heights of 16.2 k_BT, 11.1 k_BT are obtained for $W^T=W_{VEB}$, and $\gamma=1$ mN/m and 0.1 mN/m,

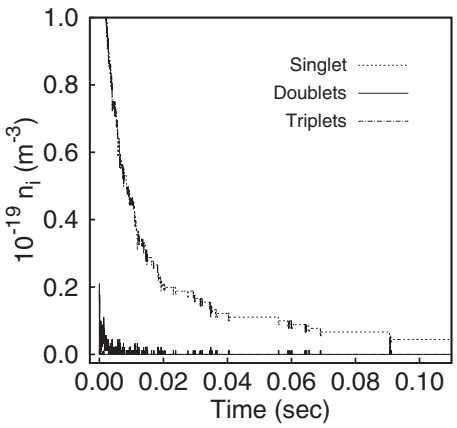

FIG. 18. Evolution of i-aggregates for a system composed by deformable droplets of initial size $a=100$ nm and $W^T=W_{VE}$ ($\gamma=0.1$ mN/m).

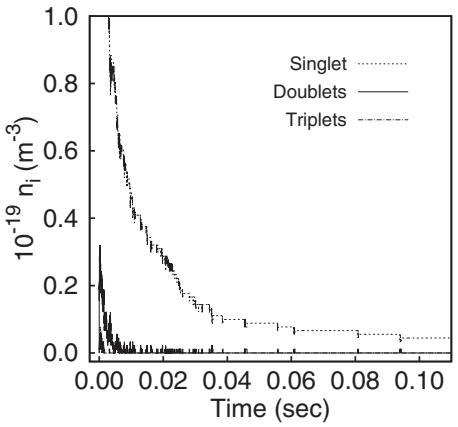

FIG. 19. Evolution of i-aggregates for a system composed by deformable droplets of initial size $a=100$ nm in absence of bending energy (and $W^T=W_{VE}$, $\gamma=1$ mN/m).

respectively. In the case of $W^T=W_{VE}$, the barrier height is equal to 5.1 k_BT for $\gamma=1$ mN/m. No barrier is observed for $\gamma=0.1$ mN/m. In Fig. 15 the potential of interaction between two droplets of $a=1$ μm is shown. In this case, the van der Waals interaction prevails. The maximum of the potential occurs at negative values in all cases. Barrier heights of 18 k_BT and 3.5 k_BT are observed for $W^T=W_{VEB}$, and $\gamma=1$ and 0.1 mN/m, respectively. A barrier height of 5.4 k_BT is obtained for $W^T=W_{VE}$, and $\gamma=1$ mN/m. No barrier was observed for $\gamma=0.1$ mN/m.

Figures 16 and 17 show the results of the simulations for $a=100$ nm, $W^T=W_{VE}$ ($\gamma=0.1$ mN/m). In the absence of a repulsive barrier, the system of deformable droplets behaves very similar to the one of non-deformable droplets. The number of particles n_{part} (Fig. 16) and aggregates n_{agg} (Fig. 17) decrease in a Smoluchowskian fashion in both cases. The number of aggregates is essentially equal to the number of single particles since the particles coalesce as soon as they flocculate. The number of doublets is small and decays very rapidly as can be observed in Fig. 18. The number of higher aggregates is negligible. Similar results are obtained for $W^T=W_{VE}(\gamma=1$ mN/m), where a small repulsive barrier exists (Fig. 19).

In order to characterize the destabilization process, a mixed average rate was computed using the formula of

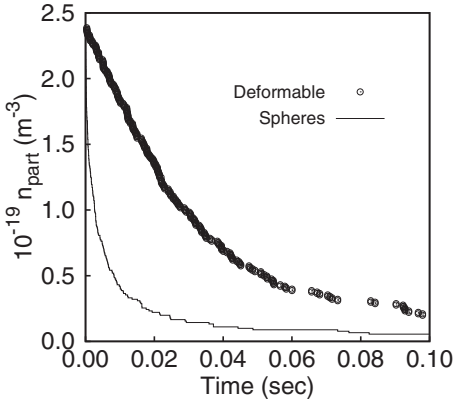

FIG. 20. Time evolution of n_{part} for a system composed of an initial droplet radius $a=100$ nm and $\gamma=0.1$ mN/m ($W^T=W_{VEB}$).

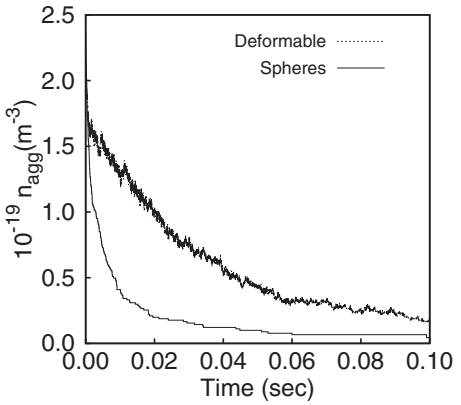

FIG. 21. Time evolution of n_{agg} for a system composed of an initial droplet radius $a=100$ nm and $\gamma=0.1$ mN/m ($W^T=W_{VEB}$).

Smoluchowski: $k_d=1/n_0t_{1/2}$. For spherical drops of 100 nm, $k_d=2.6\times10^{-17}$ m^3/s. In the case of deformable drops $k_d=2.4\times10^{-17}$ m^3/s for $\gamma=0.1$ mN/m, and 1.8×10^{-17} m^3/s for $\gamma=1$ mN/m.

When the bending potential is included in the simulations, the size of the repulsive barrier increases considerably. Figure 20 shows the results of the simulations for the case of $a=100$ nm, $W^T=W_{VEB}$ ($\gamma=0.1$ mN/m). This system shows a barrier height of 11.1 k_BT. This barrier slows down the variation of the number of particles and aggregates causing significant differences between the behavior of deformable drops and spherical particles (Fig. 21). The system of deformable drops shows the formation of doublets, triplets and even quadruplets (Fig. 22). However, the total number of aggregates does not decrease according to the equation of Smoluchowski. Using the value of $t_{1/2}$ to estimate k_d, a value of 1.9×10^{-18} m^3/s ($\gamma=0.1$ mN/m) was obtained. A similar tendency with more pronounced differences between spheres and deformable droplets is obtained for $W^T=W_{VEB}$ ($\gamma=1$ mN/m)-not shown. In the latter case $k_d=3.5\times10^{-19}$ m^3/s.

The kinetic constants for micron-sized spherical and deformable droplets are similar to systems composed of nanometric droplets ($a=100$ nm) in the absence of a strong repulsive barrier ($W^T=W_{VE}$, $\gamma=1$ mN/m). For the deformable case, a destabilization rate of $k_d\approx2\times10^{-17}$ m^3/s was obtained. On the other hand, the inclusion of the bending potential ($W^T=W_{VEB}$, $\gamma=1$ mN/m) promotes a significant degree of aggregation. In this case, the evolution of the aggregates shown in Fig. 23 is considerably slower than the one of the 100-nm particle system ($=1.9\times10^{-18}$ m^3/s). Notice also, that the curves of singlets, doublets and triplets are more clearly defined, and do not oscillate frequently as their 100 nm analogous (Fig. 24). This indicates that the flocs formed between micron-size drops are stable. This is probably due to the profound depth of the secondary minimum (-23.7 k_BT) in comparison to the one of 100-nm particles -2.65 k_BT ($W^T=W_{VEB}$, $\gamma=0.1$ mN/m). The lack of frequent oscillation also illustrates that the Brownian contribution is less important in the movement of micron size drops than in the case of small nanometer particles.

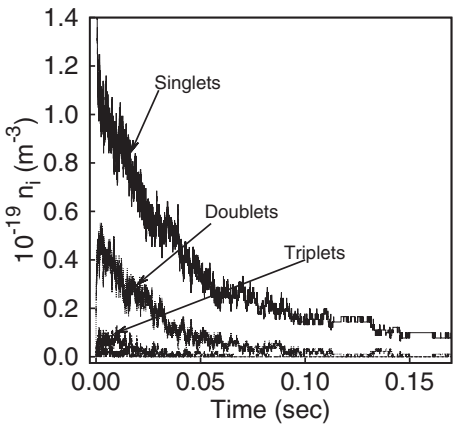

FIG. 22. Time evolution of i-aggregates for a system composed of an initial droplet radius $a=100$ nm and $\gamma=0.1$ mN/m ($W^T=W_{VEB}$).

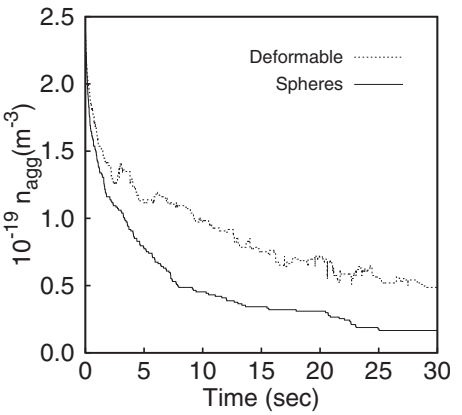

FIG. 23. Time evolution of the number of aggregates per unit volume. The initial particle size used was 1 μm and $\gamma=1$ mN/m ($W^T=W_{VEB}$).

V. CONCLUSIONS

Deformability of droplets was included in emulsion stability simulations based on a truncated spheres model. As far

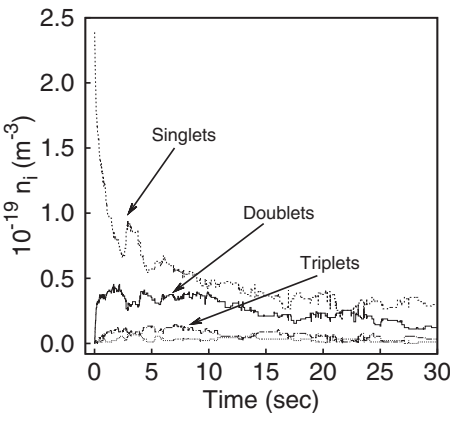

FIG. 24. Time evolution of the number of i-aggregates per unit volume of deformable droplets. The initial particle size used was 1 μm. and $\gamma=1$ mN/m ($W^T=W_{VEB}$).

as we know, these are the first simulations which account for the effect of deformability considering extensional and bending energies on the stability of emulsions. Once the droplets are deformed, it has been assumed that the coalescence time is mostly spent thinning the plane parallel film. In the absence of a significant repulsive barrier, our calculations reproduce the predictions or Ref. [17], meaning that the coalescence time of deformable and nondeformable drops is similar independently of their size (100 nm$<a<$100 μm). However, contrary to the predictions of Ref. [17], the presence of a sizeable repulsive barrier produces a maximum in the coalescence time of doublets as a function of the particle radius, which for the present potentials occurs around 3 microns. This is a consequence of the combined effect of the hydrodynamic resistance and the increment in the van der Waals attraction due to the deformation. Many particle systems were also simulated and the time evolution was analyzed by comparing deformable and nondeformable cases. Remarkable effects in aggregation processes and destabilization rates were found. The present procedure allows to include other DLVO and non DLVO interactions, and the random behavior of the film rupture process.

ACKNOWLEDGMENTS

Thanks are given to Professor Dimiter Petsev (University of New Mexico) for his helpful comments and discussions. This research was financially supported by FONACIT (Grant No. G-2005000418).

[1] T. Gurkov and E. Basheva, in *Encyclopedia of Surface and Colloid Science*, edited by A. T. Hubbard (Marcel Dekker, New York, 2002), p. 2773.
[2] J. Hofman and H. Stein, J. Colloid Interface Sci. **147**, 508 (1991).
[3] D. Petsev, in *Modern Aspects of Emulsion Science*, edited by B. P. Binks (Royal Society of Chemistry, London, 1998), Chap. 10.
[4] M. Smoluchowski, Phys. Z **17**, 557 (1916).
[5] M. Smoluchowski, Phys. Z **17**(585), 785 (1916).
[6] M. Smoluchowski, Z. Phys. Chem. **92**, 129 (1917).
[7] F. C. Collins and G. E. Kimball, J. Colloid Sci. **4**, 425 (1949).
[8] D. F. Calef and J. M. Deutch, Annu. Rev. Phys. Chem. **34**, 493 (1983).
[9] G. H. Weiss, J. Stat. Phys. **42**, 3 (1986).
[10] J. Keizer, Chem. Rev. **87**, 167 (1987).
[11] P. Debye, Trans. Electrochem. Soc. **82**, 265 (1942).
[12] N. Fuchs, Z. Phys. **89**, 736 (1934).
[13] J. M. Deutch and B. U. Felderhof, J. Chem. Phys. **59**, 1669 (1973).
[14] A. A. Ovchinnikov, S. F. Timasheff, and A. A. Belyy, *Kinetics of Diffusion Controlled Chemical Processes* (Nova Scientific, New York, 1989).
[15] B. V. Derjaguin, *Theory of Colloids and Thin Films* (Plenum Press, New York, 1989).
[16] V. M. Titulaer, Physica A **100**, 251 (1980).
[17] K. Danov, N. Denkov, D. Petsev, I. Ivanov, and R. Borwakar, Langmuir **9**, 1731 (1993).
[18] D. N. Petsev, Langmuir **16**, 2093 (2000).
[19] J. Toro-Mendoza and D. N. Petsev (to be published).
[20] G. Urbina-Villalba and M. Garcia-Sucre, Langmuir **16**, 7975 (2000).
[21] G. Urbina-Villalba, J. Toro-Mendoza, A. Lozsan, and M. Garcia-Sucre, in *Emulsions: Structure and Stability and Interactions*, edited by D. N. Petsev (Elsevier, New York, 2004), Chap. 17.
[22] I. Ivanov and D. Dimitrov, in *Thin Liquids Films*, edited by I. B. Ivanov (Marcel Dekker, New York, 1988), Chap. 7.
[23] D. Valkovska, K. Danov, and I. Ivanov, Colloids Surf., A **156**, 547 (1999).
[24] A. Nikolova and D. Exerowa, Colloids Surf., A **149**, 185 (1999).
[25] H. Zeng, B. Zhao, Y. Tian, M. Tirrel, L. Gary Leal, and J. N. IsraelachviliSoft Matter, **3**, 88 (2007).
[26] A. Sheludko, Adv. Colloid Interface Sci. **1**, 391 (1967).
[27] A. Vrij, J. Colloid Sci. **19**, 1 (1964).
[28] A. Vrij, Discuss. Faraday Soc. **42**, 23 (1966).
[29] A. Vrij and J. Overbeek, J. Am. Chem. Soc. **90**, 3074 (1968).
[30] E. Manev and A. Nguyen, Adv. Colloid Interface Sci. **114-115**, 133 (2005).
[31] A. Sharma and E. Ruckenstein, Colloid Polym. Sci. **266**, 60 (1988).
[32] R. Tsekov and E. Ruckenstein, Langmuir **9**, 3264 (1993).
[33] E. Manev and A. Nguyen, Int. J. Min. Process. **77**, 1 (2005).
[34] D. Reynolds, Philos. Trans. R. Soc. London **A177**, 157 (1886).
[35] E. Basheva, T. Gurkov, I. Ivanov, G. Bantchev, B. Campbell, and R. Borwankar, Langmuir **15**, 6764 (1999).
[36] E. Dickinson, B. S. Murray, and G. Stainsby, J. Chem. Soc., Faraday Trans. **84**, 871 (1988).
[37] I. B. Ivanov, D. S. Dimitrov, P. Somasundaran, and R. K. Jain, Chem. Eng. Sci. **40**, 137 (1985).
[38] K. Danov, D. Petsev, N. Denkov, and R. Borwankar, J. Chem. Phys. **99**, 7179 (1993).
[39] N. Denkov, D. Petsev, and K. Danov, J. Colloid Interface Sci. **176**, 189 (1995).
[40] D. Petsev, N. Denkov, and P. Kralchevsky, J. Colloid Interface Sci. **176**, 201 (1995).
[41] I. Vakarelski, A. Toritani, M. Nakayama, and K. Higashitani, Langmuir **19**, 110 (2003).
[42] P. Kralchevsky and K. Nagayama, *Particles and Fluid Interfaces and Membranes* (Elsevier, New York, 2001).
[43] P. Kralchevsky, T. Gurkov, and K. Nagayama, J. Colloid Interface Sci. **180**, 619 (1996).
[44] V. Babak, Colloids Surf., A **85**, 279 (1994).
[45] D. Woods and K. Burril, J. Electroanal. Chem. **37**, 183 (1972).
[46] R. Aveyard, B. Binks, J. Esquena, P. Fletcher, R. Buscall, and S. Davies, Langmuir **15**, 970 (1999).
[47] R. Aveyard, B. Binks, J. Esquena, P. Fletcher, P. Bault, and P. Villa, Langmuir **18**, 3487 (2002).
[48] B. Binks, W. Cho, P. Fletcher, and D. Petsev, Langmuir **16**,

1025 (2000).
[49] S. Graves, K. Meleson, J. Wilking, M. Lin, and T. Mason, J. Chem. Phys. **122**, 134703 (2005).
[50] T. Mason, S. Graves, J. Wilking, and M. Lin, J. Phys. Chem. B **110**, 22097 (2006).
[51] A. J. Castellanos S., J. Toro-Mendoza, and M. Garcia-Sucre, J. Phys. Chem. B **113**, 5891 (2009).
[52] Y. Saiki, C. Prestidge, and R. Horn, Colloids Surf., A **299**, 65 (2007).
[53] I. Ivanov, V. Danov, and P. Kralchevsky, Colloids Surf., A **152**, 161 (1999).
[54] G. Urbina-Villalba, J. Toro-Mendoza, and M. Garcia-Sucre, Langmuir **21**, 1719 (2005).
[55] A. M. Puertas, A. Fernández-Barbero, and F. de las Nieves, Comput. Phys. Commun. **121-122**, 353 (1999).
[56] A. Lozsan, M. Garcia-Sucre, and G. Urbina-Villalba, Phys. Rev. E **72**, 061405 (2005).
[57] G. Urbina-Villalba, Langmuir **20**, 3872 (2004).
[58] D. Ermak and J. McCammon, J. Chem. Phys. **69**, 1352 (1978).
[59] G. Urbina-Villalba, M. Garcia-Sucre, and J. Toro-Mendoza, Phys. Rev. E **68**, 061408 (2003).
[60] C. W. J. Beenaker and P. Mazur, Physica A **120**, 388 (1983).
[61] D. N. Petsev, in *Emulsions: Structure and Stability and Interactions*, edited by D. N. Petsev (Elsevier, New York, 2004), Chap. 8.
[62] E. Honig, G. Roebersen, and P. Wieserma, J. Colloid Interface Sci. **36**, 97 (1971).
[63] N. D. Denkov, D. Petsev, and K. D. Danov, Phys. Rev. Lett. **71**, 3226 (1993).
[64] I. Ivanov, Pure Appl. Chem. **52**, 1241 (1980).
[65] G. Urbina-Villalba, A. Lozsan, K. Rahn, and M. S. Romero-Cano, Comput. Phys. Commun. **180**, 2129 (2009).